Herd immunity thresholds for SARS-CoV-2 estimated from unfolding epidemics

Ricardo Aguas[1†], Rodrigo M. Corder[2†], Jessica G. King[3], Guilherme Gonçalves[4], Marcelo U. Ferreira[2], M. Gabriela M. Gomes[5,6*]

[1] *Centre for Tropical Medicine and Global Health, Nuffield Department of Medicine, University of Oxford, Oxford, United Kingdom.*

[2] *Instituto de Ciências Biomédicas, Universidade de São Paulo, São Paulo, Brazil.*

[3] *Institute of Evolutionary Biology, University of Edinburgh, Edinburgh, United Kingdom.*

[4] *Unidade Multidisciplinar de Investigação Biomédica, Instituto de Ciências Biomédicas Abel Salazar, Universidade do Porto, Porto, Portugal.*

[5] *Department of Mathematics and Statistics, University of Strathclyde, Glasgow, United Kingdom.*

[6] *Centro de Matemática da Universidade do Porto, Porto, Portugal.*

[†] These authors contributed equally to this work.

[*] Correspondence and requests for materials should be addressed to M.G.M.G. (email: gabriela.gomes@strath.ac.uk).

As severe acute respiratory syndrome coronavirus 2 (SARS-CoV-2) spreads, the susceptible subpopulation declines causing the rate at which new infections occur to slow down. Variation in individual susceptibility or exposure to infection exacerbates this effect. Individuals that are more susceptible or more exposed tend to be infected and removed from the susceptible subpopulation earlier. This selective depletion of susceptibles intensifies the deceleration in incidence. Eventually, susceptible numbers become low enough to prevent epidemic growth or, in other words, the herd immunity threshold is reached. Here we fit epidemiological models with inbuilt distributions of susceptibility or exposure to SARS-CoV-2 outbreaks to estimate basic reproduction numbers (R_0) alongside coefficients of individual variation (CV) and the effects of containment strategies. Herd immunity thresholds are then calculated as $1-(1/R_0)^{1/(1+CV^2)}$ or $1-(1/R_0)^{1/(1+2CV^2)}$, depending on whether variation is on susceptibility or exposure. Our inferences result in herd immunity thresholds around 10-20%, considerably lower than the minimum coverage needed to interrupt transmission by random vaccination, which for R_0 higher than 2.5 is estimated above 60%. We emphasize that the classical formula, $1-1/R_0$, remains applicable to describe herd immunity thresholds for random vaccination, but not for immunity induced by infection which is naturally selective. These findings have profound consequences for the governance of the current pandemic given that some populations may be close to achieving herd immunity despite being under more or less strict social distancing measures.

Scientists throughout the world have engaged with governments, health agencies, and with each other, to address the ongoing pandemic of coronavirus disease (COVID-19). Mathematical models have been central to important decisions concerning

contact tracing, quarantine, and social distancing, to mitigate or suppress the initial pandemic spread[1]. Successful suppression, however, may leave populations at risk to resurgent waves due to insufficient acquisition of immunity. Models have thus also addressed longer term SARS-CoV-2 transmission scenarios and the requirements for continued adequate response[2]. This is especially timely as countries apply, relax and reapply lockdown measures with varying levels of success in tackling national outbreaks.

Here we demonstrate that individual variation in susceptibility or exposure (connectivity) accelerates the acquisition of immunity in populations. More susceptible and more connected individuals have a higher propensity to be infected and thus are likely to become immune earlier. Due to this selective immunization by natural infection, heterogeneous populations require less infections to cross their herd immunity threshold (HIT) than suggested by models that do not fully account for variation. We integrate continuous distributions of susceptibility or connectivity in otherwise basic epidemic models for COVID-19 which account for realistic intervention effects and show that as coefficients of variation (CV) increase from 0 to 5, HIT declines from over 60%[3,4] to less than 10%. We then fit these models to series of daily new cases to estimate CV alongside basic reproduction numbers (R_0) and derive the corresponding HITs.

Effects of individual variation on SARS-CoV-2 transmission

SARS-CoV-2 is transmitted primarily by respiratory droplets and modelled as a susceptible-exposed-infectious-recovered (SEIR) process.

Variation in susceptibility to infection

Individual variation in susceptibility is integrated as a continuously distributed factor that multiplies the force of infection upon individuals[5] as

$$\dot{S}(x) = -\lambda(x)xS(x), \quad (1)$$

$$\dot{E}(x) = \lambda(x)x[S(x) + \sigma R(x)] - \delta E(x), \quad (2)$$

$$\dot{I}(x) = \delta E(x) - \gamma I(x), \quad (3)$$

$$\dot{R}(x) = (1 - \phi)\gamma I(x) - \sigma\lambda(x)xR(x), \quad (4)$$

where $S(x)$ is the number of individuals with susceptibility x, $E(x)$ and $I(x)$ are the numbers of individuals who originally had susceptibility x and became exposed and infectious, while $R(x)$ counts those who have recovered and have their susceptibility reduced to a reinfection factor σ due to acquired immunity. δ is the rate of progression from exposed to infectious, γ is the rate of recovery or death, ϕ is the proportion of individuals who die as a result of infection and $\lambda(x) = (\beta/N)\int[\rho E(y) + I(y)]\,dy$ is the average force of infection upon susceptible individuals in a population of size N and transmission coefficient β. Standardizing so that susceptibility distributions have mean $\int xg(x)\,dx = 1$, given a probability density function $g(x)$, the basic reproduction number is

$$R_0 = \beta\left(\frac{\rho}{\delta} + \frac{1}{\gamma}\right), \quad (5)$$

where ρ is a factor measuring the infectivity of individuals in compartment E in relation to those in I. The coefficient of variation in individual susceptibility $CV = \sqrt{\int(x-1)^2 g(x)\,dx}$ is explored as a parameter. Non-pharmaceutical interventions (NPIs) designed to control transmission typically reduce β and hence R_0. We denote the resulting controlled reproduction number by R_c. The effective reproduction

number R_{eff} is another useful indicator obtained by multiplying R_c by the susceptibility of the population, in this case written as $R_{eff}(t) = R_c(t) \int xS(x,t)\, dx/N(t)$ to emphasize its time dependence.

Top panels of Figure 1 depict model trajectories fitted to suppressed epidemics (orange) in 2 European countries (Belgium and England) assuming gamma distributed susceptibility and no reinfection ($\sigma = 0$). We estimate: R_0 rounding 5 (Belgium) and 2.9 (England); individual susceptibility CV reaching 3.9 (Belgium) and 1.5 (England); and overall intervention efficacy at maximum (typically during lockdown) being 60% (Belgium) and 54% (England). Other estimated parameters are the day when NPIs begin to affect transmission, after which we assume a linear intensification from baseline over 21 days, remaining at maximum intensity for T_{max} days and linearly lifting back to baseline over a period of T_{lift} days (both T_{max} and T_{lift} are estimated). Denoting by $d(t)$ the proportional reduction in average risk of infection due to interventions, in this case we obtain $R_c(t) = [1 - d(t)]R_0$ which is depicted for each country, alongside $R_{eff}(t)$, underneath the respective epidemic trajectories. To assess the potential for case numbers to overshoot if NPIs had not been applied, we rerun the model with $d(t) = 0$ and obtain the unmitigated epidemics (black). Further details are described in Methods.

Variation in connectivity

In a directly transmitted infectious disease, such as COVID-19, variation in exposure to infection is primarily governed by patterns of connectivity among individuals. We incorporate this in the system (Equations 1-4) assuming that individuals mix at random (but see Methods for more general formulations that enable other mixing patterns). Under random mixing and heterogeneous connectivity[6], the force of

infection is written as $\lambda(x) = (\beta/N)(\int y[\rho E(y) + I(y)]\,dy / \int y g(y)\,dy)$, the basic reproduction number is

$$R_0 = (1 + CV^2)\beta\left(\frac{\rho}{\delta} + \frac{1}{\gamma}\right), \quad (6)$$

$R_c(t)$ is as above and $R_{eff}(t)$ is derived by a more general expression given in Methods. The results from this basic variable connectivity model are shown in Extended Data Figure 1). To allow for the possibility that social distancing (d) may change not only the scale but also the shape of connectivity distributions, we consider an extended model where connectivity is reformulated as $(1 - d)[1 + (1 - d)(x - 1)]$ (Extended Data Figure 2). This does not change the way the model is written but special care is needed in analysis and interpretation to account for the dynamic contact patterns. The basic reproduction number, in particular, depends explicitly on a CV which is now dependent on social distancing.

Applying this model to the same epidemics as before we obtain the bottom panels of Figure 1. The estimated epidemiological parameters are: R_0 rounding 8.9 (Belgium) and 3.7 (England); individual connectivity CV reaching 3.9 (Belgium) and 1.6 (England); and intervention efficacy during lockdown being 45% (Belgium) and 37% (England). The reported CVs correspond to baseline contact patterns.

Comparing the two models, variation in connectivity systematically leads to higher R_0 estimates. The effect attributed to NPIs is lower in England than in Belgium. In both countries, contacts appear to reach minimal levels around lockdown in April (R_c plots), beginning to re-intensify thereafter but remaining below about half of pre-lockdown levels by the end of the data series used for model fittings (solid portions of the R_c line), consistently with the CoMix contact survey[7]. To illustrate how the

136 epidemic may unfold beyond the data used in this study we simulate a hypothetical
137 scenario whereby contacts continue to reactivate linearly until eventually reaching the
138 pre-pandemic baseline. This leads to low epidemic activity over a period that
139 coincides with the Summer months, followed by a resurge as contacts intensify. This
140 resurgence is likely to be aggravated by seasonality as the Winter approaches,
141 although seasonality has not been included in our models. The percentage of the
142 population required to be immune to curb the epidemic and prevent future waves
143 when interventions are lifted appears remarkably conserved across models: 10 vs 11%
144 (Belgium); and 27 vs 25% (England).

145 We then fit to the same data the model constrained by $CV = 0$, i.e. assuming no
146 relevant heterogeneity in susceptibility or exposure to infection. The results are shown
147 in Figure 2. In this case epidemic potential is considerably larger and hence the effect
148 attributed to NPIs to fit the data must also be larger. The percentage of the population
149 required to be immune to prevent epidemic growth when interventions are lifted rises
150 to 73% (Belgium) and 63% (England).

151 **Herd immunity thresholds**

152 Individual variation in risk of acquiring infection is under selection by the force of
153 infection, whether individual differences are due to biological susceptibility,
154 exposure, or both. The most susceptible or exposed individuals are selectively
155 removed from the susceptible pool as they become infected and eventually recover
156 (some die), resulting in decelerated epidemic growth and accelerated induction of
157 immunity in the population. In essence, the *herd immunity threshold* defines the
158 percentage of the population that needs to be immune to reverse epidemic growth and
159 prevent future waves. When individual susceptibility or connectivity is gamma-

160 distributed and mixing is random, HIT curves can be derived analytically[8] from the
161 model systems (Equations 1-4, with the respective forces of infections). In the case of
162 variation in susceptibility to infection we obtain

163 $$HIT = 1 - \left[\frac{1 - \sigma R_0}{(1-\sigma)R_0}\right]^{\frac{1}{1+CV^2}}, \quad (7)$$

164 while variable connectivity results in

165 $$HIT = 1 - \left[\frac{1 - \sigma R_0}{(1-\sigma)R_0}\right]^{\frac{1}{1+2CV^2}}. \quad (8)$$

166 In more complex cases (such as the variable connectivity with dynamic CV or
167 assortative mixing) HIT curves can be approximated numerically. Figure 3 shows the
168 expected downward trends in HIT and the sizes of the respective unmitigated
169 epidemics for SARS-CoV-2 without reinfection ($\sigma = 0$) as the coefficients of
170 variation are increased (here we adopt gamma distributions; for robustness of the
171 trends to other distributions see Gomes et al[9]). Values of R_0 and CV estimated for our
172 study countries are overlaid to mark the respective HIT and final epidemic sizes.
173 While herd immunity is expected to require 60-80% of a homogeneous population to
174 have been infected, at the cost of infecting almost the entire population if left
175 unmitigated, given an R_0 between 2.5 and 5, these percentages drop to the range 10-
176 20% when CV is roughly between 1.5 and 4.

177 When acquired immunity is not 100% effective ($\sigma > 0$) HITs are relatively higher
178 (Extended Data Figure 3). However, there is an upper bound for how much it is
179 reasonable to increase σ before the system enters a qualitatively different regime.
180 Above $\sigma = 1/R_0$ – the *reinfection threshold*[10,11]– infection becomes stably endemic

and the HIT concept no longer applies. Respiratory viruses are typically associated with epidemic dynamics below the reinfection threshold, characterized by seasonal epidemics intertwined with periods of low detection.

Individual variation in exposure, in contrast with susceptibility, accrues from complex patterns of human behaviour which have been simplified in our basic model. To explore the scope of our results we generalised the models by relaxing some key assumptions. First, we allowed connectivity distributions to change in shape (not only scale) when subject to social distancing (Figure 1, bottom panels). Second, we enable mixing to be assortative in the sense that individuals contact predominantly with those of similar connectivity (Methods). Formally, an individual with connectivity x, rather than being exposed uniformly to individuals of all connectivities y, has contact preferences described by a normal distribution on the difference $y - x$. We find this modification to have negligible effect on HIT (Extended Data Figure 4).

Herd immunity thresholds and seroprevalence at sub-national levels

As countries conduct immunological surveys to assess the extent of exposure to SARS-CoV-2 in populations it is of practical importance to understand how HIT may vary across regions. We have redesigned our analyses to address this question. Series of daily new cases in 4 European countries (Belgium, England, Portugal and Spain) were stratified by region. Fitting the models simultaneously to the multiple series enabled the estimation of local parameters (R_0 and CV) while the effects of NPIs were estimated at country level. Extended Data Figures 5-8 show how the modelled epidemics fit the regional data and include an additional metric to describe the cumulative infected percentage. These model projections are comparable to data from seroprevalence studies such as in Spain[12]. In addition to their practical utility these

205 results begin to unpack some of the variation in HIT within countries: Belgium (9.4-
206 11%), England (16-26%), Portugal (7.1-9.9%) and Spain (7.5-21%). The sub-national
207 stratification has also enabled the application of the models to countries where the
208 epidemic was sufficiently asynchronous across regions to compromise the ability of
209 the models to fit the aggregate data (Portugal and Spain).

210 **Discussion**

211 The concept of *herd immunity* was developed in the context of vaccination
212 programs[13,14]. Defining the percentage of the population that must be immune to
213 cause infection incidences to decline, HITs constitute useful targets for vaccination
214 coverage. In idealized scenarios of vaccines delivered at random and individuals
215 mixing at random, HITs are given by a simple formula $(1 - 1/R_0)$ which, in the case
216 of SARS-CoV-2, suggests that 60-80% of randomly chosen subjects of the population
217 would need be immunized to halt spread considering estimates of R_0 between 2.5 and
218 5. This formula does not apply to infection-induced immunity because natural
219 infection does not occur at random. Individuals who are more susceptible or more
220 exposed are more prone to be infected and become immune, providing greater
221 community protection than random vaccination[15]. In our model, the HIT declines
222 sharply when coefficients of variation increase from 0 to 2 and remains below roughly
223 20% for more variable populations. The magnitude of the decline depends on what
224 property is heterogeneous and how it is distributed among individuals, but the
225 downward trend is robust as long as susceptibility or exposure to infection are
226 variable (Figure 3 and Extended Data Figures 4) and acquired immunity is efficacious
227 enough to keep transmission below the reinfection threshold (Extended Data Figure
228 3).

Several candidate vaccines against SARS-CoV-2 are showing promising safety and immunogenicity in early-phase clinical trials[16,17], although it is not yet known how this will translate into effective protection. We note that the reinfection threshold[10,11] informs not only the requirements on naturally acquired immunity but, similarly, it sets a target for how efficacious a vaccine needs to be in order to effectively interrupt transmission. Specifically, given an estimated value of R_0 we should aim for a vaccine efficacy of $1 - 1/R_0$ (60% or 80% if R_0 is 2.5 or 5, respectively), which seems to be materialising according to preliminary results from phase 3 trials.

Heterogeneity in the transmission of respiratory infections has traditionally focused on variation in exposure summarized into age-structured contact matrices. Besides overlooking differences in susceptibility given exposure, the aggregation of individuals into age groups reduces coefficients of variation. We calculated CV for the landmark POLYMOD matrices[18,19] and obtained values between 0.3 and 0.5. Recent studies of COVID-19 integrated contact matrices with age-specific susceptibility to infection (structured in three levels)[20] or with social activity (three levels also)[21] which, again, resulted in coefficients of variation less than unity. We show that models with coefficients of variation of this magnitude would appear to differ only moderately from homogeneous approximations when compared with our estimates, which are consistently above 1 in England and above 2 in Belgium, Portugal and Spain. In contrast with reductionist procedures that aim to reconstruct variation from correlate markers left on individuals (such as antibody or reactive T cells for susceptibility, or contact frequencies for exposure), we have embarked on a holistic approach designed to infer the whole extent of individual variation from the imprint it leaves on epidemic trajectories. Our estimates are therefore expected to be higher and should ultimately be confronted with more direct measurements as these

become available. Adam at et[22] conducted a contact tracing study in Hong Kong and estimated a coefficient of variation of 2.5 for the number of secondary infections caused by individuals, attributing 80% of transmission to 20% of cases. This statistical dispersion has been interpreted as reflecting a common pattern of contact heterogeneity which has been corroborated by studies that specifically measure mobility[23]. According to our inferences, 20% of individuals may be responsible for 47-94% infections depending on model and country. In parallel, there is accumulating evidence of individual variation in the immune system′s ability to control SARS-CoV-2 infection following exposure[24,25]. While our inferences serve their purpose of improving accuracy in model predictions, diverse studies such as these are necessary for developing interventions targeting individuals who may be at higher risk of being infected and propagating infection in the community.

Country-level estimates of R_0 reported here (Figures 1, 2) are in the range 3-5 when individual variation in susceptibility is factored and 4-9 when accounting for variation in connectivity. The homogeneous version of our models would have estimated R_0 around 2.7 and 3.7, in line with other studies[26]. Estimates for England suggest lower baseline R_0 and lower CV in comparison with Belgium. The net effect is a slightly higher HIT in England which nevertheless we estimate around 25-27% depending on characteristics of the individual variation. NPIs reveal less impact when heterogeneity is contemplated (37-60%), appearing to inflate and agree with Flaxman et al[26] when homogeneity assumptions are made (66-78%), although this does not affect the HIT which relates to pre-pandemic societies.

More informative than reading these numbers, however, is to look at simulated projections of how cases may unfold over future months (Figures 1, 2). In both

278 countries, when individual variation is considered, we foresee HIT being achieved
279 and the COVID-19 epidemic being mostly resolved by the end of 2020. Under the
280 homogeneous approximation, however, epidemic potential appears to justify
281 considerations of second lockdowns to flatten epidemic curves. Determining the level
282 of confidence on either scenario is highly relevant to policy decisions and hence of
283 central importance to public health. According to the Akaike information criterion
284 (Extended Data Table 5) data favours the models that account for individual variation
285 and a more natural resolution for the pandemic. Models that account for individual
286 variation in susceptibility score particularly well and amongst those that account for
287 variation in exposure those that allow this variation to reduce with social distancing
288 perform better.

289 Looking back, we conclude that NPIs had a crucial role in halting the growth of the
290 initial wave between February and April irrespective of individual variation. Although
291 the most extreme lockdown strategies may not be sustainable for longer than a month
292 or two, they proved effective at preventing overshoot, keeping cases within health
293 system capacities, and may have done so without impairing the development of herd
294 immunity.

295

296 1. Ferguson, N. M., et al. Impact of non-pharmaceutical interventions (NPIs) to reduce
297 COVID-19 mortality and healthcare demand (Imperial College COVID-19 Response
298 Team, 2020). 10.25561/77482.
299 2. Kissler, S. M., Tedijanto, C., Goldstein, E., Grad, Y. H. & Lipsitch, M. Projecting the
300 transmission dynamics of SARS-CoV-2 through the postpandemic period. *Science* **368**,
301 860-868 (2020).

3. Wu, J. T., Leung, K. & Leung, G. M. Nowcasting are forecasting the potential domestic and international spread of the 2019-nCov outbreak originating in Wuhan, China: a modelling study. *Lancet* **395**, 689-697 (2020).

4. Kwok, K. O., Lai, F., Wei, W. I., Wong, S. Y. S. & Tang, J. Herd immunity – estimating the level required to halt the COVID-19 epidemics in affected countries. *J. Infect.* **80**, e32-e33 (2020).

5. Diekmann, O., Heesterbeek, J. A. P. & Metz, J. A. J. On the definition and computation of the basic reproduction ratio R_0 in models for infectious diseases in heterogeneous populations. *J. Math. Biol.* **28**, 365-382 (1990).

6. Pastor-Satorras, R. & Vespignani, A. Epidemic dynamics and endemic states in complex networks. *Phys. Rev. E* **63**, 066117 (2001).

7. Jarvis, C. I., et al. Quantifying the impact of physical distance measures on the transmission of COVID-19 in the UK. *BMC Medicine* **18**, 206 (2020).

8. Montalbán, A., Corder, R. M. & Gomes, M. G. M. Herd immunity under individual variation and reinfection. *arXiv* 200800098v2. (2020).

9. Gomes, M. G. M., et al. Individual variation in susceptibility or exposure to SARS-CoV-2 lowers the herd immunity threshold. *medRvix* 10.1101/2020.04.27.20081893 (2020).

10. Gomes, M. G. M., White, L. J. & Medley, G. F. Infection, reinfection, and vaccination under suboptimal immune protection: Epidemiological perspectives. *J. Theor. Biol.* **228**, 539-549 (2004).

11. Gomes, M. G. M., Gjini, E., Lopes, J. S., Souto-Maior, C. & Rebelo, C. A theoretical framework to identify invariant thresholds in infectious disease epidemiology. *J. Theor. Biol.* **395**, 97-102 (2016).

12. Pollán, M., et al. Prevalence of SARS-CoV-2 in Spain (ENE-COVID): a nationwide, population-based seroepidemiological study. *Lancet* 10.1016/s0140-6736(20)31483-5 (2020).

13. Gonçalves, G. Herd immunity: recent uses in vaccine assessment. *Expert Rev. Vaccines* **7**, 1493-1506 (2008).

14. Fine, P., Eames, K. & Heymann, D. L. "Herd immunity": a rough guide, *Clin. Infect. Dis.* **52**, 911-916 (2011).

15. Ferrari, M. J., Bansal, S., Meyers, L. A. & Bjornstad, O. N. Network frailty and the geometry of herd immunity. *Proc. R. Soc. B* **273**, 2743-2748 (2006).

16. Folegatti, P. M., et al. Safety and immunogenicity of the ChAdOx1 nCoV-19 vaccine against SARS-CoV-2: a preliminary report of a phase 1/2, single-blind, randomised controlled trial. *Lancet* 10.1016/S0140-6736(20)31604-4 (2020).

17. Zhu, F.-C., et al. Immunogenicity and safety of a recombinant adenovirus type-5-vectored COVID-19 vaccine in healthy adults aged 18 years or older: a randomised, double-blind, placebo-controlled, phase 2 trial. *Lancet* 10.1016/S0140-6736(20)31611-1 (2020).

18. Mossong, J., et al. Social contacts and mixing patterns relevant to the spread of infectious diseases. *PLOS Med*. **5**, e74 (2008).

19. Prem, K., Cook, A. R. & Jit, M. Projecting social contact matrices in 152 countries using contact surveys and demographic data. *PLOS Comput. Biol.* **13**, e1005697 (2017).

20. Zhang, J., et al. Changes in contact patterns shape the dynamics of the COVID-19 outbreak in China. *Science* **368**, 1481-1486 (2020).

21. Britton, T., Ball, F. & Trapman, P. A mathematical model reveals the influence of population heterogeneity on herd immunity to SARS-CoV-2. *Science* 10.1126/science.abc6810 (2020).

22. Adam, D., et al. Clustering and superspreading potential of severe acute respiratory syndrome coronavirus 2 (SARS-CoV-2) infections in Hong Kong. 10.21203/rs.3.rs-29548/v1

23. Eubank, S., et al. Modelling disease outbreaks in realistic urban social networks. *Nature* **429**, 180-184 (2004).

355 24. Grifoni, A., et al. Targets of T cell responses to SARS-CoV-2 coronavirus in humans
356 with COVID-19 disease and unexposed individuals. *Cell* **181**, 1489-1501.e15 (2020).
357 25. Le Bert, N., et al. SARS-CoV-2-specific T cell immunity in cases of COVID-19 and
358 SARS, and uninfected controls. *Nature* 10.1038/s41586-020-2550-z (2020).
359 26. Flaxman, S., et al. Estimating the effects of non-pharmaceutical interventions on
360 COVID-19 in Europe. *Nature* 10.1038/s41586-020-2405-7 (2020).
361

362

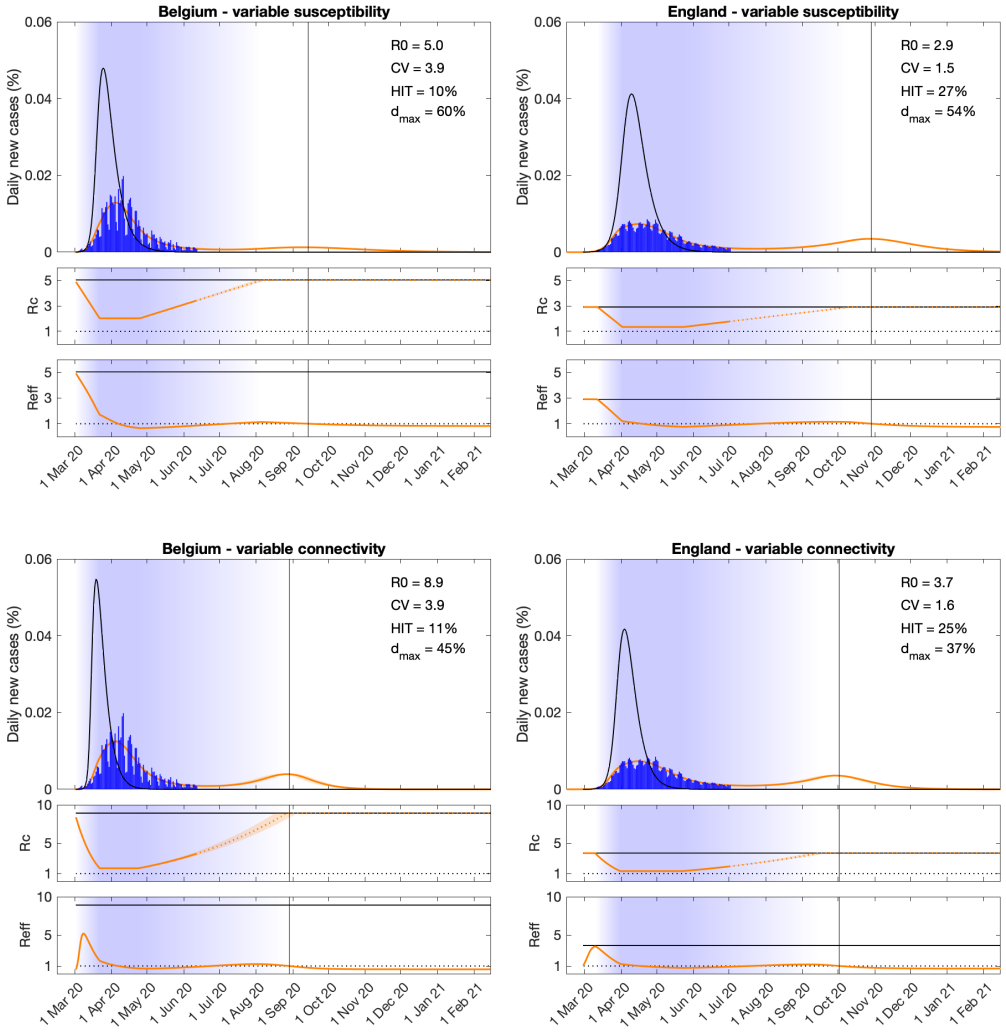

363

364 **Fig. 1| SARS-CoV-2 transmission with individual variation.** Variation in
365 susceptibility (top panels); variation in connectivity (CV reducing in proportion to
366 social distancing) (bottom panels). Susceptibility or connectivity factors implemented
367 as gamma distributions. Suppressed wave and subsequent dynamics in Belgium and
368 England (orange). Estimated epidemic in the absence of interventions revealing
369 overshoot (black). Blue bars are daily new cases. Controlled (R_c) and effective (R_{eff})
370 reproduction numbers are displayed on shallow panels underneath the main plots.
371 Blue shades represent social distancing (intensity reflected in R_c trends and shade
372 density). R_c values in the dotted portion of the orange lines do not interfere with the
373 fittings and are only used to illustrate how the epidemic may unfold beyond the data
374 analysed here. Consensus parameter values (Methods): $\delta = 1/4$ per day; $\gamma = 1/4$ per
375 day; and $\rho = 0.5$. Fraction of infected individuals identified as positive (reporting
376 fraction): 0.06 (Belgium); 0.024 (England). Basic reproduction number, coefficients
377 of variation and social distancing parameters estimated by Bayesian inference as
378 described in Methods (estimates in Extended Data Tables 1 and 3). Curves represent
379 mean model predictions from 10^4 posterior samples. Orange shades represent 95%
380 credible intervals. Vertical lines represent the expected time when herd immunity
381 threshold will be achieved.
382

383

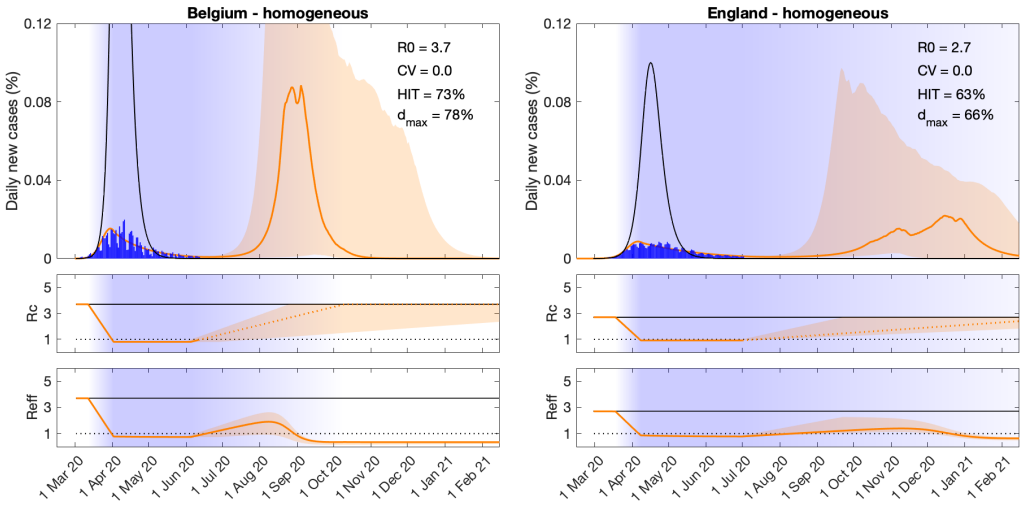

384

385 **Fig. 2| SARS-CoV-2 transmission in homogeneous populations.** Suppressed wave
386 and subsequent dynamics in Belgium and England (orange). Estimated epidemic in
387 the absence of interventions revealing overshoot (black). Blue bars are daily new
388 cases. Controlled (R_c) and effective (R_{eff}) reproduction numbers are displayed on
389 shallow panels underneath the main plots. Blue shades represent social distancing
390 (intensity reflected in R_c trends and shade density). R_c values in the dotted portion of
391 the orange lines do not interfere with the fittings and are only used to illustrate how
392 the epidemic may unfold beyond the data analysed here. Consensus parameter values
393 (Methods): $\delta = 1/4$ per day; $\gamma = 1/4$ per day; and $\rho = 0.5$. Fraction of infected
394 individuals identified as positive (reporting fraction): 0.06 (Belgium); 0.024
395 (England); 0.09 (Portugal); 0.06 (Spain). Basic reproduction number, coefficients of
396 variation and social distancing parameters estimated by Bayesian inference as
397 described in Methods (estimates in Extended Data Table 4). Curves represent mean
398 model predictions from 10^4 posterior samples. Orange shades represent 95% credible
399 intervals.
400

401

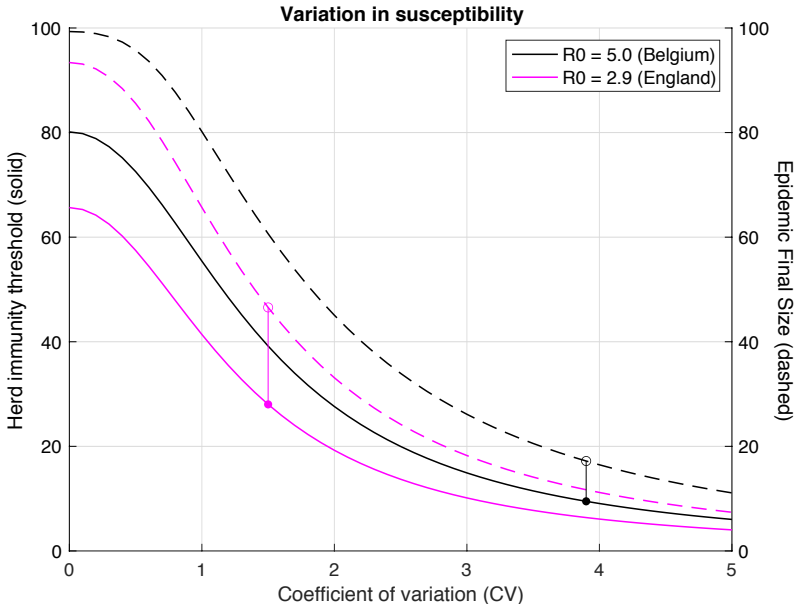

402

403

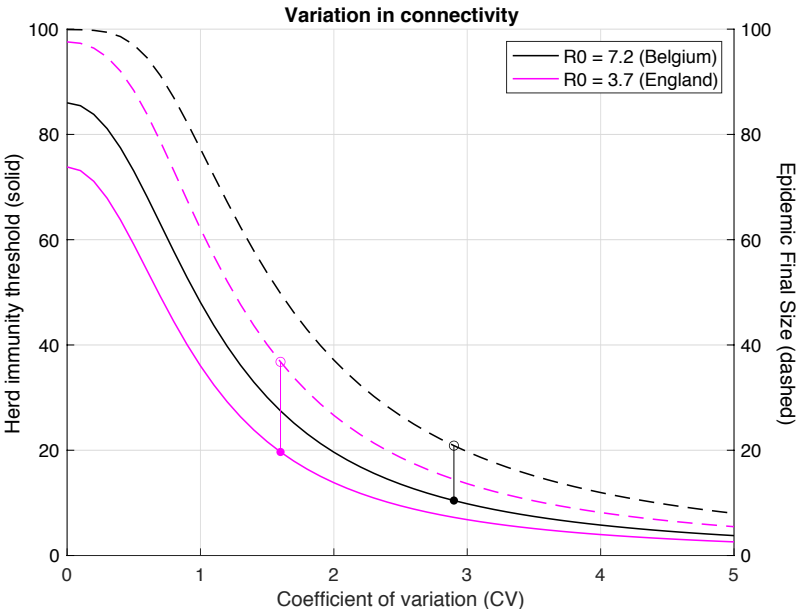

404

405 **Fig. 3| Herd immunity threshold with gamma-distributed susceptibility or**
406 **exposure to infection.** Curves generated with the SEIR model (Equation 1-4)
407 assuming values of R_0 estimated for the study countries (Extended Data Tables 1 and
408 2) assuming gamma-distributed: susceptibility (top); connectivity (bottom) with
409 constant CV. Herd immunity thresholds (solid curves) are calculated according to the
410 formula $1-(1/R_0)^{1/(1+CV^2)}$ for heterogeneous susceptibility and $1-$
411 $(1/R_0)^{1/(1+2CV^2)}$ for heterogeneous connectivity. Final sizes of the corresponding
412 unmitigated epidemics are also shown (dashed).

METHODS

Model structure and underlying assumptions

The model presented here is a differential equation SEIR model, where susceptible individuals become exposed at a rate that depends on their susceptibility, the number of potentially infectious contacts they engage in, and the total number of infectious people in the population per time unit. Upon exposure, individuals enter an asymptomatic incubation phase, during which they slowly become infectious[27-30]. Thus, infectivity of exposed individuals is made to be $1/2$ of that of infectious ones ($\rho = 0.5$). After a few days, individuals develop symptoms – on average 4 days after the exposure to the virus ($\delta = 1/4$) – and thus become fully infectious[31-33]. They recover, i.e., they are no longer infectious 4 days after that ($\gamma = 1/4$), on average[34].

Efficacy of acquired immunity

We conducted the core of our analysis under the assumption that no reinfection occurs after recovery due to acquired immunity ($\sigma = 0$). To analyse the sensitivity of these results to leakage in immune response ($\sigma > 0$) we calculated herd immunity thresholds (HIT) as a function of coefficients of variation (CV) for different values of σ. The results displayed in Extended Data Figure 3 confirm the expectation that as the efficacy of acquired immunity decreases (σ increases) larger percentages of the population are infected before herd immunity is reached. Less intuitive is that there is an upper bound for how much it is reasonable to increase σ before the system enters a qualitatively different regime – the reinfection threshold[10,11] ($\sigma = 1/R_0$) – above which infection becomes stably endemic and the notion of herd immunity threshold

435 no longer applies. Respiratory viruses are typically associated with epidemics
436 dynamics below the reinfection threshold.

437 *Effective reproduction number*

438 The effective reproduction number (R_{eff}, also denoted by R_e or R_t by other authors)
439 is a time-dependent quantity which we calculate as the incidence of new infections
440 divided by the total number of active infections (affected by ρ for individuals in E)
441 multiplied by the average duration of infection (also affected by ρ for individuals in
442 E)

443 $$R_{eff}(t) = \frac{\int \lambda(x,t)x[S(x,t) + \sigma R(x,t)]\, dx}{\int \rho E(x,t) + I(x,t)\, dx} \left(\frac{\rho}{\delta} + \frac{1}{\gamma}\right). \quad (9)$$

444 *Assortative mixing*

445 In the main text we assumed random mixing among individuals, but human
446 connectivity patterns are assortative due societal structures and human behaviours. To
447 explore the sensitivity of our results to deviations from random mixing, we develop
448 an extended formalism that allows individuals to connect preferentially with those
449 with similar connectivity, formally $\lambda(x) =$
450 $(\beta/N)(\int y\, h(y-x)[\rho E(y) + I(y)]\, dy / \int y g(y)\, dy)$, where $h(y-x)$ is a normal
451 distribution on the difference between connectivity factors (Extended Data Figure 2).

452 *Non-pharmaceutical interventions*

453 We implemented non-pharmaceutical interventions (NPI) as a gradual decrease in
454 viral transmissibility in the population and thus a lowering of the controlled and
455 effective reproduction numbers (R_c and R_{eff}). Once containment measures are put in

place in each country, we postulate it takes 21 days until the maximum effectiveness of social distancing measures is reached, approximately linearly. In the simulations presented throughout we have held this condition (maximum "lockdown" efficacy) for T_{max} days, where T_{max} is estimated for each study country in countrywide analyses and fixed at 30 in regional analyses. Eventually, lockdowns were lifted and social distancing measures progressively relaxed. This relaxation is implemented linearly over a period of T_{lift} days, which is also estimated. We note however that the estimation of epidemiological parameters is not affected by the shape assumed for the relaxation of interventions beyond the date of the last data point (June 11th in Belgium and July 1st in England). In particular, assuming that social distancing measures remained constant from these dates onwards, for example, would make no difference to the estimated parameters.

Bayesian Inference

The model laid out above is amenable to theoretical exploration as presented in the main manuscript and provides a perfect framework for inference. Fundamentally, to be able to reproduce the inception of any epidemic, we would need to estimate when local transmission started to occur (t_0), and the pace at which individuals infected each other in the very early stages of the epidemic (R_0). All countries, to different extents and at different timepoints of the epidemic, enforced some combination of social distancing measures. To fully understand the interplay between herd immunity and the impact of NPIs, we then set out to estimate the time at which social distancing measures started to have an impact on daily incidence (t_0^d), what their maximum efficacy (d_{max}) was and how long it lasted (T_{max}), a parameter used to determine the rate at which contacts resume as restrictions are lifted (T_{lift}, which more specifically

480 represents the time it would take to reach pre-pandemic contact intensity should the
481 lifting of restricting have linear effect), the basic reproduction number (R_0) and what
482 the underlying variance in heterogeneity is for susceptibility or exposure to infection.

483 In order to preserve identifiability, we made two simplifying assumptions: (*i*) the
484 fraction of infectious individuals reported as COVID-19 cases (reporting fraction) is
485 constant throughout the study period and is comparable between countries
486 proportionally to the number of tests performed per person; (*ii*) local transmission
487 starts (t_0) when countries/regions report 1 case per 5 million population in one day.
488 To calculate the reporting rates, we used the Spanish national serological survey[12] as a
489 reference and divided the total number of reported cases up to May 11th by the
490 estimated number of people that had been exposed to the virus. This gives us a
491 reporting rate for Spain around 6%. Unfortunately, there are no other national
492 serological surveys that could inform the proportion of the population infected in
493 other countries, so we had to extrapolate the reporting rate for those. Assuming the
494 reporting rate is highly dependent on the testing effort employed in each country,
495 reflected in the number of tests per individual, we estimate the reporting rate by
496 scaling the reporting rate recorded in Spain according to the ratio of PCR tests per
497 person in other countries relative to the Spanish reference of 0.9 tests per thousand
498 people (https://ourworldindata.org/coronavirus-testing). This produced estimated case
499 reporting rates (ratio of reported cases to infections) of 9% for Portugal, 6% for
500 Belgium (and Spain) and 2.4% for England.

501 Whist national case and mortality data is easily available for most countries, more
502 spatially resolute data is difficult to find in the public domain. Thus, we restricted our
503 analysis to countries for which disaggregated regional case data was easily available.

We collected the data at two time points. First, we compiled all available data from the day the countries started reporting COVID-19 cases to the initial collection date (May 20th) and later collated available data from May 21st to July 10th.

Parameter estimation was performed with the software MATLAB, using PESTO (Parameter EStimation Toolbox)[35], and assuming the reported case data can be accurately described by a Poisson process. We first fixed the beginning of local transmission (parameter t_0) in each data series as the day in which reported cases surpassed 1 in 5 million individuals. Next, we optimized the model for the set of parameters $\theta = \{R_0, CV, t_0^d, d_{max}, T_{max}, T_{lift}\}$ by maximizing the logarithm of the likelihood (LL) (Equation 10) of observing the daily reported number of cases in each country $D = \{(k, \tilde{y}_k)\}_{k=0}^{n}$:

$$LL(\theta|D) = -\sum_{k=1}^{n} y(k,\theta) + \left(\sum_{k=1}^{n} \tilde{y}(k)\ \ln\left(y(k,\theta)\right)\right) - ln\left(\prod_{k=1}^{n} \tilde{y}(k)!\right) \quad (10)$$

in which $y(k,\theta)$ is the simulated model output number of COVID-19 cases at day k (with respect to t_0), and n is the total number of days included in the analysis for each country.

To ensure that the estimated maximum is a global maximum, we performed 50 multi-starts optimizations, and selected the combination of parameters resulting in the maximal Loglikelihood as a starting point for 10^4 Markov Chain Monte-Carlo iterations. From the resulting posterior distributions, we extract the median estimates for each parameter and the respective 95% credible intervals for the set of parameters. We used uniformly distributed priors with ranges {1-9, 0.0025-8,1-60, 0-0.7,1-90,60-1000}.

When fitting the model to disaggregated data, we follow the procedure outlined above but fix $T_{max} = 30$ days, $T_{lift} = 120$ days and estimate region-specific R_0 and CV, with common t_0^d and d_{max}.

The countrywide fitting procedure was applied to 2 countries (Belgium and England) and repeated for each of the 4 model variants considered here (homogeneous, heterogeneous susceptibility, heterogeneous connectivity with constant CV, and heterogeneous connectivity with CV reducing in proportion to social distancing). Our study included two more countries (Portugal and Spain), where countrywide analyses could not be performed due to the epidemic being geographically desynchronised. We implemented stratified analyses on all 4 countries. In the fitting procedures using sub-national data, we assumed regions had the same start date for interventions that mitigate transmission (t_0^d), and that these measures produced the same maximum impact on transmission (d_{max}) everywhere. Thus, the only region-specific parameters to be estimated are $\{R_{0_i}, CV_i\}$. Parameter estimates obtained from each of the model variants are displayed in Extended Data Table 1 (heterogeneity in susceptibility), Extended Data Table 2 (heterogeneity in connectivity with constant CV), Extended Data Table 3 (heterogeneity in connectivity with dynamic CV) and Extended Data Table 4 (homogeneous model), are comparable to those obtained in other studies[7,26,37-40]. Finally, we apply the Akaike information criterion (AIC) for each estimation procedure to inform on the quality of each model's fit to the datasets of reported cases (Extended Data Table 5). In all cases, heterogeneous models are preferred over the homogeneous approximation. The three heterogeneous models are roughly equally well supported by the data used in this study. Further research should complement this with discriminatory data types and hybrid models to enable the integration of different forms of individual variation.

Data and code availability

Datasets are publicly available at the respective national ministry of health websites (41-45). Core models implemented in MATLAB available from:

https://github.com/mgmgomes1/covid

27. Wei, W. E., et al. Presymptomatic Transmission of SARS-CoV-2 — Singapore, January 23–March 16, 2020. MMWR Morb Mortal Wkly Rep [Internet]. 2020 Apr 10 [cited 2020 May 4];69(14):411–5. Available from: http://www.cdc.gov/mmwr/volumes/69/wr/mm6914e1.htm?s_cid=mm6914e1_w
28. To, K. K. W., et al. Temporal profiles of viral load in posterior oropharyngeal saliva samples and serum antibody responses during infection by SARS-CoV-2: an observational cohort study. *Lancet Infect. Dis.* **20**, 565-74 (2020).
29. Arons, M. M., et al. Presymptomatic SARS-CoV-2 Infections and Transmission in a Skilled Nursing Facility. *N. Engl. J. Med.* **382**, 2081-2090 (2020).
30. He, X., et al. Temporal dynamics in viral shedding and transmissibility of COVID-19. *Nat. Med.* **26**, 672-675 (2020).
31. Lauer, S. A., et al. The Incubation Period of Coronavirus Disease 2019 (COVID-19) From Publicly Reported Confirmed Cases: Estimation and Application. *Ann. Intern. Med.* **172**, 577-582 (2020).
32. Li, Q., et al. Early transmission dynamics in Wuhan, China, of novel coronavirus-infected pneumonia. *N. Engl. J. Med.* **382**, 1199-1207 (2020).
33. Zhang, J., et al. Evolving epidemiology and transmission dynamics of coronavirus disease 2019 outside Hubei province, China: A descriptive and modelling study. *Lancet Infect. Dis.* **20**, 793-802 (2020).
34. Nishiura, H., Linton, N. M. & Akhmetzhanov, A. R. Serial interval of novel coronavirus (COVID-19) infections. *Int. J. Infect. Dis.* **93**, 284-6 (2020).

576 35. Stapor, P., et al. PESTO: Parameter EStimation TOolbox. *Bioinformatics* **34**, 705-707
577 (2018).
578 36. Prem, K., et al. The effect of control strategies to reduce social mixing on outcomes of
579 COVID-19 epidemic in Wuhan, China: a modelling study. *Lancet Public Health* **5**, e261-
580 e270.
581 37. Tian, H., et al. An investigation of transmission control measures during the first 50 days
582 of the COVID-19 epidemic in China. *Science* **368**, 638-642.
583 38. Kucharski, A. J., et al. Effectiveness of isolation, testing, contact tracing and physical
584 distancing on reducing transmission of SARS-CoV-2 in different settings: a
585 mathematical modelling study. *Lancet Infect. Dis.* 10.1016/s1473-3099(20)30457-6
586 (2020).
587 39. Salje, H., et al. Estimating the burden of SARS-CoV-2 in France. *Science* **369**, 208-211
588 (2020).
589 40. Di Domenico, L., Pullano, G., Sabbatini, C. E., Boelle, P.-Y. & Colizza, V. Expected
590 impact of lockdown in Île-de-France and possible exit strategies. *medRxiv*
591 10.1101/2020.04.13.20063933 (2020).
592 41. https://ourworldindata.org/coronavirus-testing#source-information-country-by-
593 country. Accessed on July 10th 2020.
594 42. https://cnecovid.isciii.es/covid19.
595 43. https://covid-19.sciensano.be/nl/covid-19-epidemiologische-situatie.
596 44. https://covid19.min-saude.pt/ponto-de-situacao-atual-em-portugal.
597 45. https://coronavirus.data.gov.uk.

598

599 **Acknowledgements**

600 We thank Jan Hasenauer and Antonio Montalbán for helpful discussions concerning
601 statistical inference and mathematics, respectively. R.M.C. and M.U.F. receive

602 scholarships from the Conselho Nacional de Desenvolvimento Científico e
603 Tecnológio (CNPq), Brazil.

604

605 **Author contributions**

606 M.G.M.G. conceived the study. R.A. and R.M.C. and M.G.M.G. performed the
607 analyses. All authors interpreted the data and wrote the paper.

608

609 **Competing interests**

610 The authors declare no competing interests.

611

612

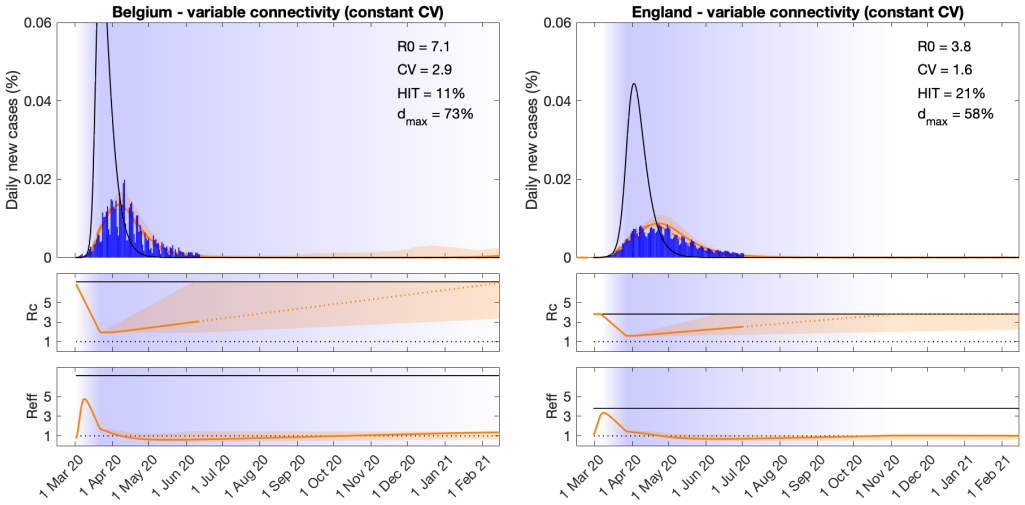

613

614 **Extended Data Fig. 1| SARS-CoV-2 transmission with individual variation in**
615 **connectivity.** Variation in connectivity (constant CV). Connectivity factors
616 implemented as gamma distributions. Suppressed wave and subsequent dynamics in
617 Belgium and England (orange). Estimated epidemic in the absence of interventions
618 revealing overshoot (black). Blue bars are daily new cases. Controlled (R_c) and
619 effective (R_{eff}) reproduction numbers are displayed on shallow panels underneath the
620 main plots. Blue shades represent social distancing (intensity reflected in R_c trends
621 and shade density). R_c values in the dotted portion of the orange lines do not interfere
622 with the fittings and are only used to illustrate how the epidemic may unfold beyond
623 the data analysed here. Consensus parameter values (Methods): $\delta = 1/4$ per day; $\gamma =$
624 $1/4$ per day; and $\rho = 0.5$. Fraction of infected individuals identified as positive
625 (reporting fraction): 0.06 (Belgium); 0.024 (England). Basic reproduction number,
626 coefficients of variation and social distancing parameters estimated by Bayesian
627 inference as described in Methods (estimates in Extended Data Table 2). Curves
628 represent mean model predictions from 10^4 posterior samples. Orange shades
629 represent 95% credible intervals. Vertical lines represent the expected time when herd
630 immunity threshold will be achieved.
631

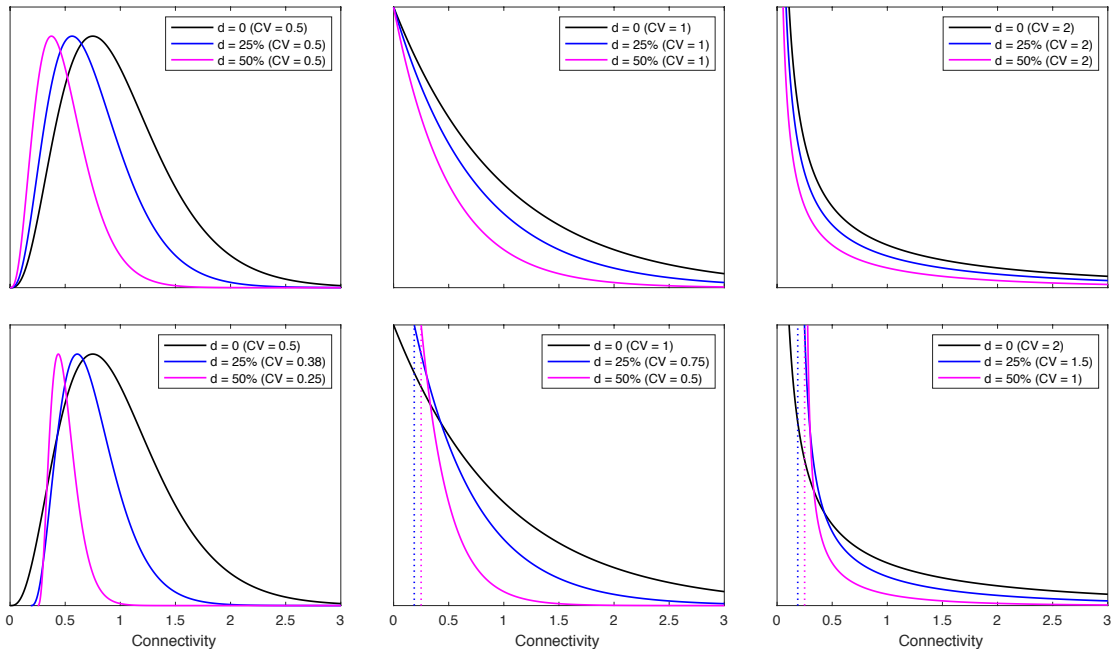

Extended Data Fig. 2| Connectivity distributions with reducing coefficient of variation in proportion to social distancing. Individual variation in connectivity is originally implemented as a gamma distribution of mean 1 parameterised by the coefficient of variation (CV) (black). Social distancing is initially implemented as a reduction in connectivity by the same factor to every individual, from x to $(1-d)x$ (top panels). A more general formulation where CV may reduce with social distancing is implemented by modifying x to $(1-d)[1+(1-d)(x-1)]$ (bottom panels).

643

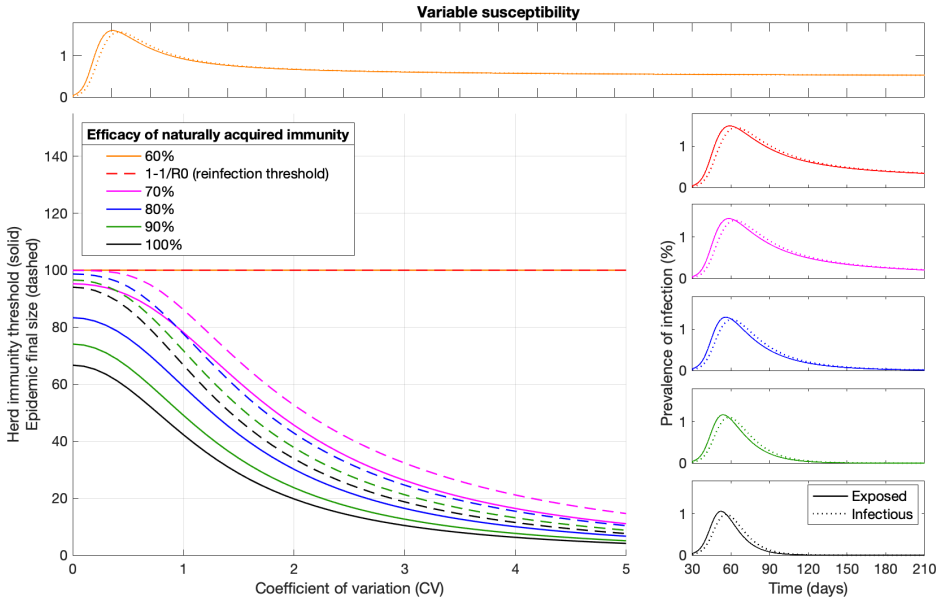

644

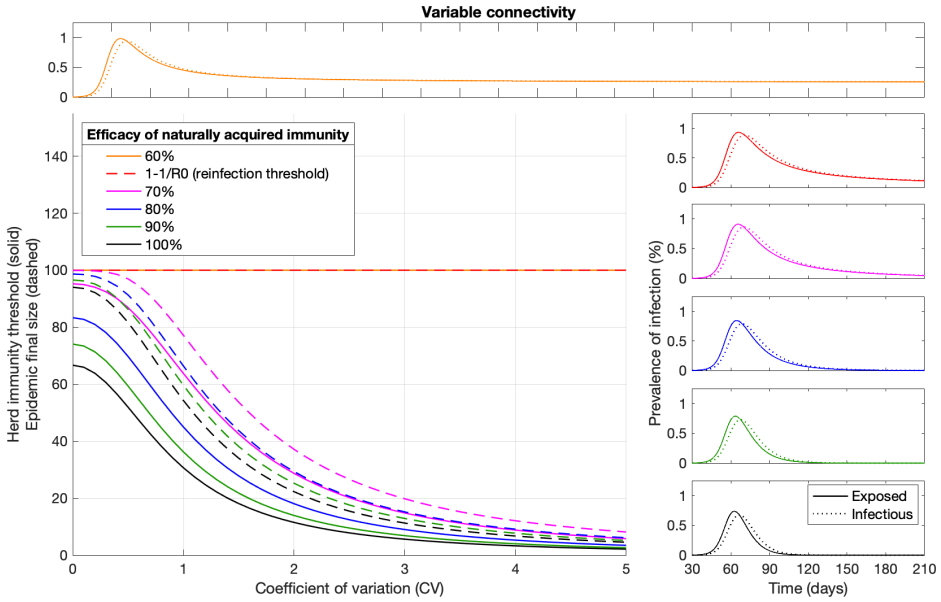

645

646 **Extended Data Fig. 3| Herd immunity threshold and epidemic final size with**
647 **reinfection.** Curves in the main panels generated with the SEIR model (Equation 1-4)
648 assuming $R_0 = 3$ and gamma-distributed susceptibility (top) or connectivity (bottom)
649 with constant CV. Efficacy of acquired immunity is captured by a reinfection
650 parameter σ, potentially ranging between $\sigma = 0$ (100% efficacy) and $\sigma = 1$ (0
651 efficacy). This illustration depicts final sizes of unmitigated epidemics and associated
652 HIT curves for 6 values of σ: $\sigma = 0$ (black); $\sigma = 0.1$ (green); $\sigma = 0.2$ (blue); $\sigma = 0.3$
653 (magenta); $\sigma = 1/3$ (red); and $\sigma = 0.4$ (orange);. Above $\sigma = 1/R_0$ (reinfection
654 threshold (Gomes et al 2004; 2016)) the infection becomes stably endemic and there
655 is no herd immunity threshold. Representative epidemics of the regime $\sigma \leq 1/R_0$ are
656 shown on the right while the regime $\sigma > 1/R_0$ is illustrated on top. All depicted
657 dynamics are based on the rightmost CVs represented on the main panel.
658

659

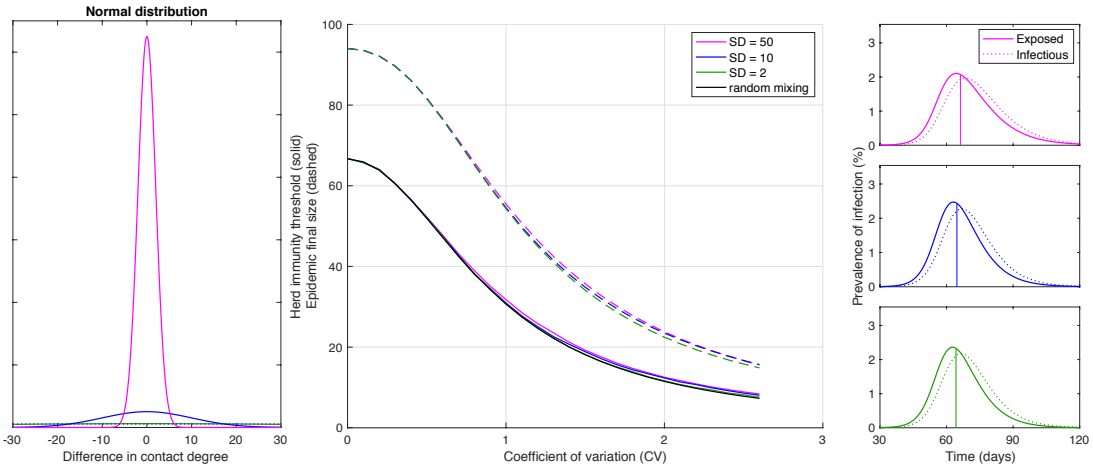

660

661 **Extended Data Fig. 4| Herd immunity threshold and epidemic final size with**
662 **gamma-distributed exposure to infection and assortative mixing.** Curves in
663 central panel generated with the SEIR model (Equation 1-4) assuming $R_0 = 3$ and
664 gamma-distributed connectivity. Assortative mixing is implemented by imposing a
665 normal distribution for contact preferences such that individuals contact preferentially
666 with those with the similar contact degree (left). This illustration used normal
667 distributions with standard deviation $SD = 50$ (green); $SD = 10$ (blue); and $SD = 2$
668 (magenta). More assortative mixing leads to more skewed epidemics. Herd immunity
669 thresholds were calculated numerically as the percentage of the population no longer
670 susceptible when new outbreaks are effectively prevented (approximately when the
671 exposed fraction crosses the peak in the absence of mitigation). Final sizes of the
672 corresponding unmitigated epidemics are also shown. Representative epidemics are
673 depicted on the right based on the rightmost CVs represented on the main panel (with
674 vertical lines marking the point when herd immunity is achieved).
675

676

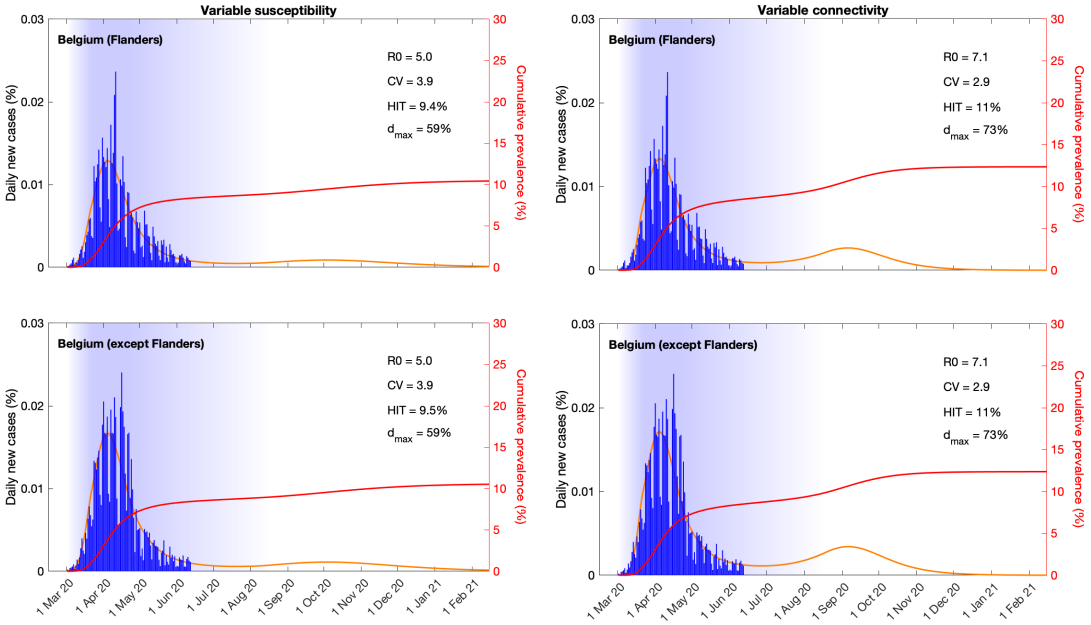

677 **Extended Data Fig. 5| SARS-CoV-2 transmission at subnational levels in Belgium.**
678 Suppressed wave and subsequent dynamics in Flanders and the rest of Belgium, with
679 individual variation in susceptibility (left) or exposure (right). Blue bars are daily new
680 cases. Shades represent social distancing (intensity reflected in shade density).
681 Susceptibility or exposure factors implemented as gamma distributions. Consensus
682 parameter values (Methods): $\delta = 1/4$ per day; $\gamma = 1/4$ per day; and $\rho = 0.5$.
683 Fraction of infected individuals identified as positive (reporting fraction): 0.06. Basic
684 reproduction number, coefficients of variation and social distancing parameters
685 estimated by Bayesian inference as described in Methods (estimates in Extended Data
686 Table 1 and 2). Curves represent mean model predictions from 10^4 posterior samples.
687 Orange shades represent 95% credible intervals. Red curves represent cumulative
688 infected percentages.
689

690

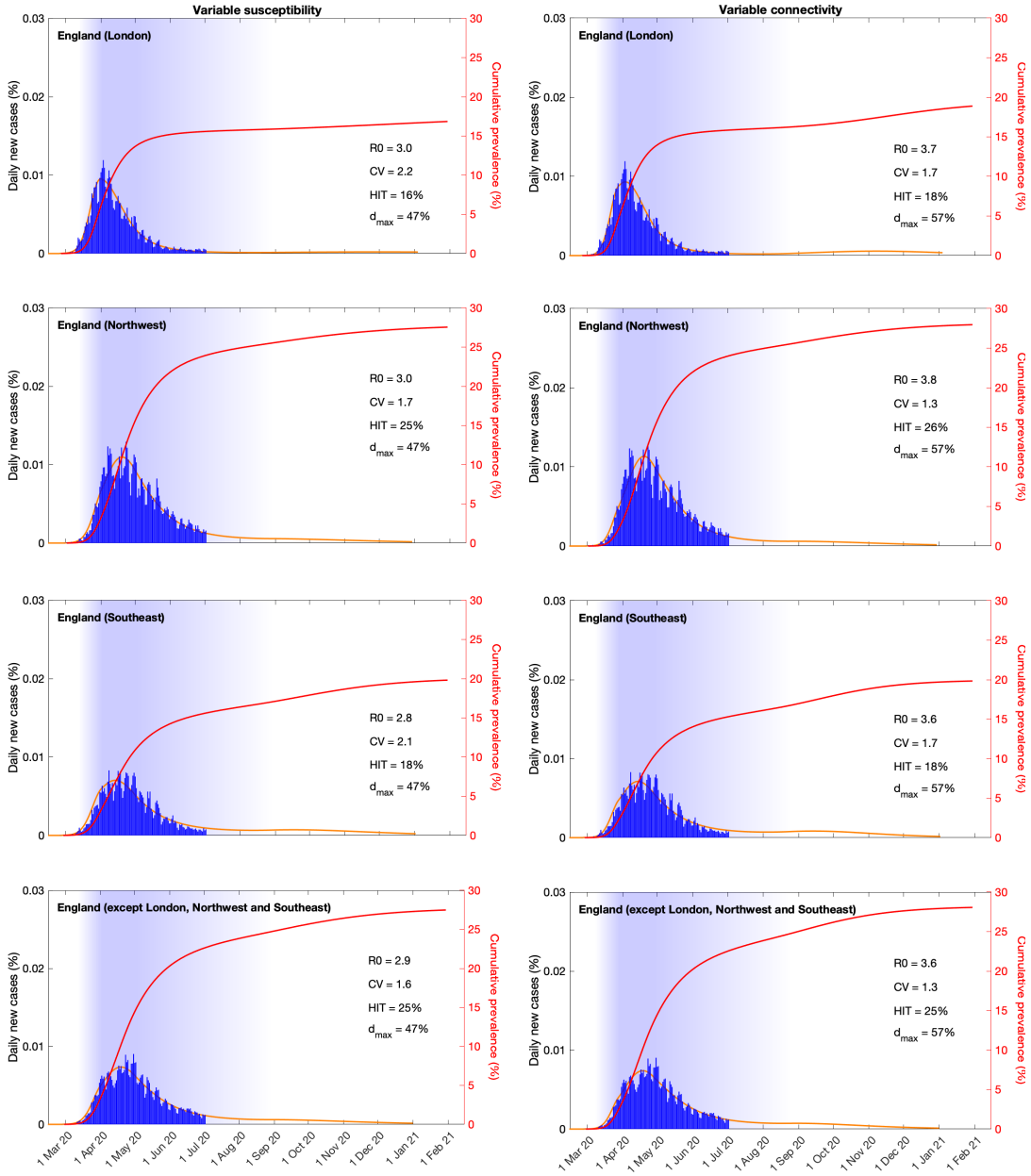

691 **Extended Data Fig. 6| SARS-CoV-2 transmission at subnational levels in England.**
692 Suppressed wave and subsequent dynamics in London, Northwest, Southeast and the
693 rest of England, with individual variation in susceptibility (left) or exposure (right).
694 Blue bars are daily new cases. Shades represent social distancing (intensity reflected
695 in shade density). Susceptibility or exposure factors implemented as gamma
696 distributions. Consensus parameter values (Methods): $\delta = 1/4$ per day; $\gamma = 1/4$ per
697 day; and $\rho = 0.5$. Fraction of infected individuals identified as positive (reporting
698 fraction): 0.024. Basic reproduction number, coefficients of variation and social
699 distancing parameters estimated by Bayesian inference as described in Methods
700 (estimates in Extended Data Table 1 and 2). Curves represent mean model predictions
701 from 10^4 posterior samples. Orange shades represent 95% credible intervals. Red
702 curves represent cumulative infected percentages.
703

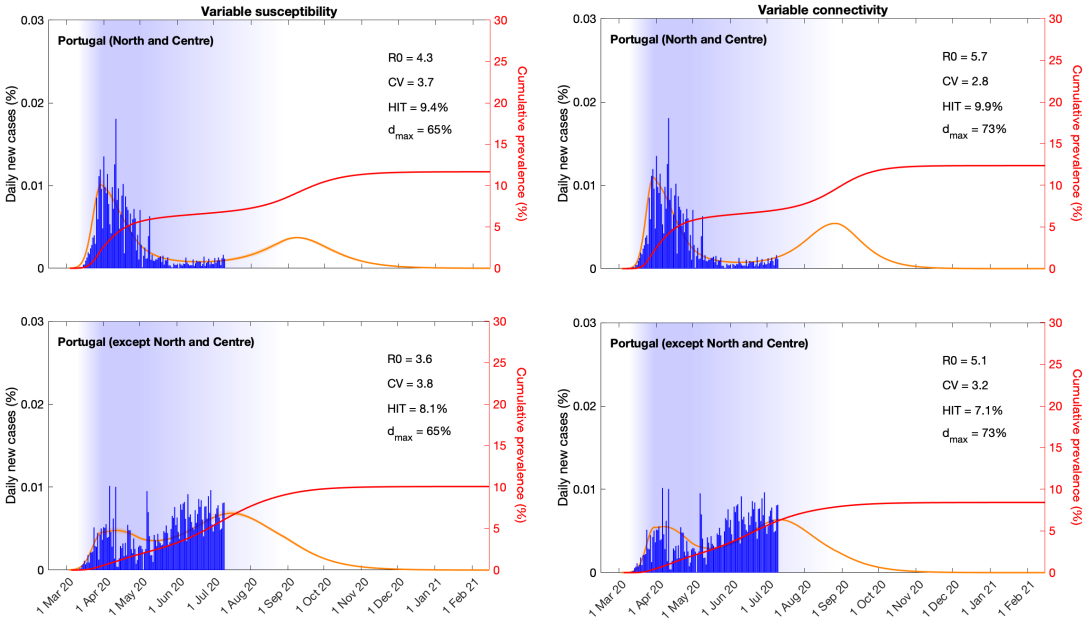

Extended Data Fig. 7| SARS-CoV-2 transmission at subnational levels in Portugal. Suppressed wave and subsequent dynamics in the North and Centre regions versus the rest of Portugal, with individual variation in susceptibility (left) or exposure (right). Blue bars are daily new cases. Shades represent social distancing (intensity reflected in shade density). Susceptibility or exposure factors implemented as gamma distributions. Consensus parameter values (Methods): $\delta = 1/4$ per day; $\gamma = 1/4$ per day; and $\rho = 0.5$. Fraction of infected individuals identified as positive (reporting fraction): 0.09. Basic reproduction number, coefficients of variation and social distancing parameters estimated by Bayesian inference as described in Methods (estimates in Extended Data Table 1 and 2). Curves represent mean model predictions from 10^4 posterior samples. Orange shades represent 95% credible intervals. Red curves represent cumulative infected percentages.

718

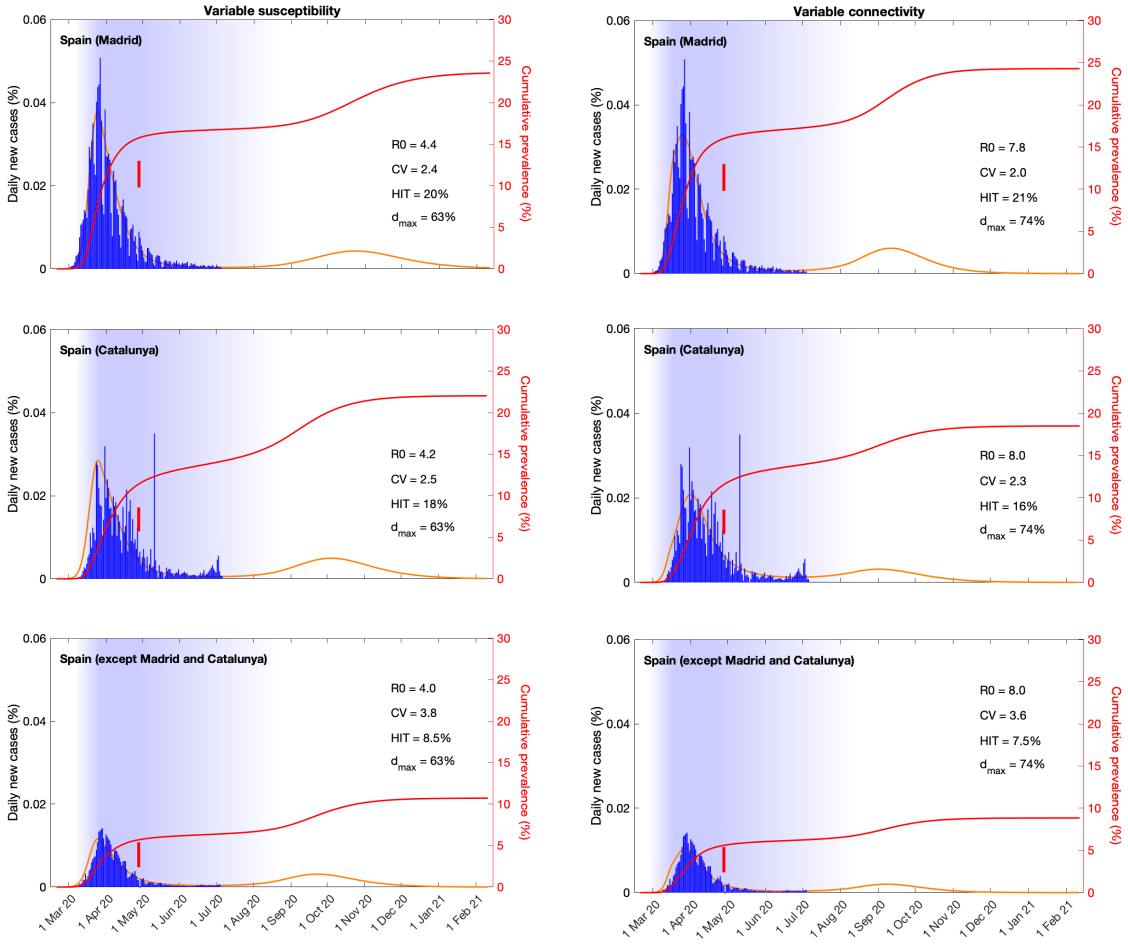

719 **Extended Data Fig. 8| SARS-CoV-2 transmission at subnational levels in Spain.**
720 Suppressed wave and subsequent dynamics in Madrid, Catalunya and the rest of
721 Spain, with individual variation in susceptibility (left) or exposure (right). Blue bars
722 are daily new cases. Shades represent social distancing (intensity reflected in shade
723 density). Susceptibility or exposure factors implemented as gamma distributions.
724 Consensus parameter values (Methods): $\delta = 1/4$ per day; $\gamma = 1/4$ per day; and $\rho =$
725 0.5. Fraction of infected individuals identified as positive (reporting fraction): 0.06.
726 Basic reproduction number, coefficients of variation and social distancing parameters
727 estimated by Bayesian inference as described in Methods (estimates in Extended Data
728 Table 1 and 2). Curves represent mean model predictions from 10^4 posterior samples.
729 Orange shades represent 95% credible intervals. Red curves represent cumulative
730 infected percentages and vertical red segments mark seroprevalences (95% CI)
731 according to a recent study[12].
732

Extended Data Table 1| Estimated parameters for heterogeneous susceptibility model. Estimates generated from model fit to the national datasets are in the grey shaded rows. The remaining rows provide the region-specific estimates. Best parameter estimates are presented as a bold median bounded by the lower and upper ends for the 95% credible interval. Model runs are initiated on the day ($\boldsymbol{t_0}$) when reported cases surpassed 1 in 5 million individuals: Belgium (day 1); England (day 29); Portugal (day 3); Spain (day 8).

Country/Region	R_0			CV			$1-d_{max}$			t_0^d		
Belgium	5.01	**5.03**	5.05	3.84	**3.87**	3.89	0.40	**0.40**	0.40	1.00	**1.02**	1.08
Flanders	4.96	**5.00**	5.02	3.89	**3.91**	3.93	0.41	**0.41**	0.41	1.00	**1.02**	1.15
Rest	4.97	**5.01**	5.03	3.87	**3.89**	3.91						
Portugal												
North/Centre	4.27	**4.32**	4.36	3.69	**3.72**	3.74	0.34	**0.35**	0.35	7.51	**7.73**	8.00
Rest	3.54	**3.58**	3.61	3.72	**3.76**	3.79						
Spain												
Madrid	4.38	**4.39**	4.39	2.37	**2.37**	2.38	0.37	**0.37**	0.37	16.40	**16.41**	16.44
Catalunya	4.20	**4.21**	4.21	2.49	**2.50**	2.50						
Rest	3.96	**3.97**	3.97	3.80	**3.81**	3.82						
England	2.90	**2.91**	2.92	1.54	**1.54**	1.55	0.46	**0.46**	0.46	42.03	**42.19**	42.41
London	2.95	**2.96**	2.96	2.24	**2.24**	2.24	0.52	**0.53**	0.53	41.35	**41.51**	41.64
NorthWest	3.03	**3.04**	3.05	1.66	**1.67**	1.68						
SouthEast	2.80	**2.81**	2.82	2.07	**2.07**	2.07						
Rest	2.88	**2.88**	2.89	1.64	**1.64**	1.65						

Extended Data Table 2| Estimated parameters for heterogeneous connectivity model (constant CV). Estimates generated from model fit to the national datasets are in the grey shaded rows. The remaining rows provide the region-specific estimates. Best parameter estimates are presented as a bold median bounded by the lower and upper ends for the 95% credible interval. Model runs are initiated on the day ($\boldsymbol{t_0}$) when reported cases surpassed 1 in 5 million individuals: Belgium (day 1); England (day 29); Portugal (day 3); Spain (day 8).

Country/Region	R_0			CV			$1-d_{max}$			t_0^d		
Belgium	7.13	**7.15**	7.16	2.87	**2.87**	2.87	0.27	**0.27**	0.28	1.00	**1.00**	1.02
Flanders	7.09	**7.11**	7.13	2.86	**2.87**	2.89	0.27	**0.27**	0.28	1.00	**1.01**	1.03
Rest	7.11	**7.13**	7.15	2.86	**2.87**	2.89						
Portugal												
North/Centre	5.06	**5.08**	5.09	3.24	**3.24**	3.24	0.25	**0.25**	0.25	7.21	**7.22**	7.24
Rest	5.68	**5.69**	5.69	2.79	**2.81**	2.83						
Spain												
Madrid	7.81	**7.83**	8.82	1.98	**1.99**	2.06	0.24	**0.26**	0.26	5.38	**7.02**	7.06
Catalunya	8.00	**8.02**	9.00	2.33	**2.34**	2.43						
Rest	7.97	**7.99**	8.96	3.58	**3.59**	3.72						
England	3.81	**3.82**	3.84	1.55	**1.55**	1.55	0.42	**0.42**	0.42	36.38	**37.49**	36.54
London	3.70	**3.70**	3.71	1.69	**1.69**	1.70	0.43	**0.43**	0.43	37.50	**37.52**	37.55
NorthWest	3.83	**3.83**	3.84	1.32	**1.32**	1.32						
SouthEast	3.58	**3.59**	3.59	1.66	**1.67**	1.68						
Rest	3.60	**3.60**	3.61	1.30	**1.31**	1.31						

Extended Data Table 3| Estimated parameters for heterogeneous connectivity model (dynamic CV). Estimates generated from model fit to the national datasets are in the grey shaded rows. The remaining rows provide the region-specific estimates. Best parameter estimates are presented as a bold median bounded by the lower and upper ends for the 95% credible interval. Model runs are initiated on the day ($\boldsymbol{t_0}$) when reported cases surpassed 1 in 5 million individuals: Belgium (day 1); England (day 29); Portugal (day 3); Spain (day 8).

Country/Region	R_0			CV			$1-d_{max}$			t_0^d		
Belgium	8.88	**8.91**	8.94	3.89	**3.92**	3.95	0.55	**0.55**	0.55	1.00	**1.00**	1.00
Flanders	8.78	**8.82**	8.86	3.98	**4.00**	4.02	0.56	**0.56**	0.56	1.00	**1.01**	1.04
Rest	8.82	**8.86**	8.89	3.98	**4.00**	4.02						
Portugal												
North/Centre	6.65	**6.72**	6.80	3.75	**3.78**	3.81	0.56	**0.57**	0.57	5.84	**6.02**	6.19
Rest	5.98	**6.05**	6.13	4.09	**4.14**	4.19						
Spain												
Madrid	6.19	**6.20**	6.21	2.43	**2.43**	2.44	0.57	**0.57**	0.57	13.80	**13.81**	13.83
Catalunya	6.30	**6.32**	6.33	2.61	**2.62**	2.62						
Rest	6.34	**6.35**	6.36	3.80	**3.81**	3.82						
England	3.67	**3.67**	3.68	1.56	**1.57**	1.57	0.63	**0.63**	0.63	39.81	**39.82**	39.83
London	3.78	**3.79**	3.80	1.99	**2.00**	2.01	0.67	**0.67**	0.67	39.06	**39.20**	39.28
NorthWest	3.91	**3.92**	3.94	1.64	**1.65**	1.66						
SouthEast	3.67	**3.69**	3.70	1.89	**1.89**	1.90						
Rest	3.64	**3.65**	3.66	1.58	**1.58**	1.59						

Extended Data Table 4| Estimated parameters for the homogenous model.
Estimates generated from model fit to the national datasets are in the grey shaded rows. The remaining rows provide the region-specific estimates. Best parameter estimates are presented as a bold median bounded by the lower and upper ends for the 95% credible interval. Model runs are initiated on the day ($\boldsymbol{t_0}$) when reported cases surpassed 1 in 5 million individuals: Belgium (day 1); England (day 29); Portugal (day 3); Spain (day 8).

Country/Region	R_0			$1-d_{max}$			t_0^d		
Belgium	3.683	**3.698**	3.712	0.218	**0.219**	0.220	11.948	**12.054**	12.173
Flanders	3.235	**3.239**	3.308	0.208	**0.212**	0.213	16.324	**17.039**	17.064
Rest	3.235	**3.238**	3.307						
Portugal									
North/Centre	3.542	**3.578**	3.608	0.343	**0.345**	0.348	7.514	**7.725**	7.999
Rest	4.274	**4.321**	4.361						
Spain									
Madrid	4.113	**4.116**	4.120	0.111	**0.111**	0.112	20.000	**20.000**	20.000
Catalunya	4.208	**4.214**	4.218						
Rest	3.735	**3.751**	3.752						
England	2.690	**2.703**	2.708	0.339	**0.339**	0.340	48.091	**48.155**	48.244
London	2.307	**2.308**	2.310	0.359	**0.360**	0.360	54.577	**54.578**	54.578
NorthWest	2.602	**2.603**	2.604						
SouthEast	2.368	**2.370**	2.371						
Rest	2.502	**2.503**	2.504						

Extended Data Table 5| Model selection criteria. Displays the maximum Loglikelihood obtained for each combination of model and data partitioning for each country, as well as the Akaike information criterion. Models are labelled by a sort name as follows: homog (homogenous); hetsus (heterogeneity in susceptibility); hetcon (heterogeneity in connectivity with constant CV); hetdyn (heterogeneity in connectivity with dynamic CV).

Country	*Model*	*LL*	*AIC*
Countrywide Data			
England	homog	1.6765E+06	-3.3529E+06
	hetsus	1.6793E+06	-3.3585E+06
	hetcon	1.6785E+06	-3.3571E+06
	hetdyn	1.6790E+06	-3.3579E+06
Belgium	homog	3.3204E+05	-6.6407E+05
	hetsus	3.3325E+05	-6.6649E+05
	hetcon	3.3269E+05	-6.6537E+05
	hetdyn	3.3278E+05	-6.6554E+05
Regional Data			
Portugal	homog	3.36E+05	-6.73E+05
	hetsus	3.55E+05	-7.11E+05
	hetcon	3.55E+05	-7.10E+05
	hetdyn	3.55E+05	-7.11E+05
Spain	homog	1.87E+06	-3.75E+06
	hetsus	1.96E+06	-3.91E+06
	hetcon	1.96E+06	-3.91E+06
	hetdyn	1.47E+06	-2.95E+06
England	homog	2.59E+06	-5.18E+06
	hetsus	2.63E+06	-5.25E+06
	hetcon	2.62E+06	-5.25E+06
	hetdyn	2.62E+06	-5.25E+06
Belgium	homog	3.74E+05	-7.48E+05
	hetsus	3.78E+05	-7.56E+05
	hetcon	3.78E+05	-7.55E+05
	hetdyn	3.78E+05	-7.55E+05